Draft version June 21, 2012
Preprint typeset using LaTeX style emulateapj v. 5/2/11

DISTRIBUTION OF MAXIMAL LUMINOSITY OF GALAXIES IN THE SLOAN DIGITAL SKY SURVEY

M. Taghizadeh-Popp [1], K. Ozogány [2], Z. Rácz [2], E. Regoes [3], A.S. Szalay [1]

(Dated: June 21, 2012)
Draft version June 21, 2012

ABSTRACT

Extreme value statistics (EVS) is applied to the distribution of galaxy luminosities in the Sloan Digital Sky Survey (SDSS). We analyze the DR8 Main Galaxy Sample (MGS), divided into red and blue subsamples, as well as the Luminous Red Galaxies (LRG). Maximal luminosities are sampled from batches consisting of elongated pencil beams in the radial direction of sight. For the MGS, results suggest a small and positive tail index ξ, effectively ruling out the possibility of having a finite maximum cutoff luminosity, and implying that the luminosity distribution function may decay as a power law at the high luminosity end. Assuming, however, $\xi = 0$, a non-parametric comparison of the maximal luminosities with the Fisher-Tippett-Gumbel distribution (limit distribution for variables distributed by the Schechter fit) indicates a good agreement provided uncertainties arising both from the finite batch size and from the batch size distribution are accounted for. For a volume limited sample of LRGs, results show that they can be described as being the extremes of a luminosity distribution with an exponentially decaying tail, having had these uncertainties considered as well.

Subject headings: methods: statistical — Galaxies: statistics — galaxies: general — galaxies: luminosity function — galaxies: fundamental parameters

1. INTRODUCTION

Extreme value statistics is a powerful tool for analyzing the behavior of the tails of distributions. It is well-known that the distribution of extreme values for a sample of N–i.i.d. (independent, identically distributed) random variables converge (as $N \to \infty$) to a few limiting distributions depending on the tail behavior of the parent population (Fisher-Tippett-Gumbel, Weibull, Fisher-Tippett-Frechet (Gumbel 1958; Galambos 1978)). However, the onset of this finite sample size scaling behavior is quite slow, and therefore requires very large samples to converge. This is the primary reason why astronomy has seen few applications of EVS to date.

The emergence of dedicated wide angle galaxy surveys, such as SDSS (Stoughton et al. 2002), has made possible an increase in statistics, making galaxy samples in the SDSS redshift survey just large enough to attempt an analysis of the finite sample size scaling for all galaxies. Here we chose to study the distribution of maximal luminosities of galaxies, since the galaxy luminosity distribution per volume or luminosity function (LF) is one of the most basic statistic measured in galaxy surveys. This function has been well described by a gamma distribution or so-called Schechter function (Schechter 1976), functionally similar (and motivated by) the theoretically derived Press-Schechter formula (Press & Schechter 1974), with a power law distribution at the faint end and an exponentially falling tail at the bright end. When galaxies are grouped according to their morphologies, their respective LFs seem to belong to different classes, including bell-shaped distributions as well as gamma functions of different shape and scale parameters (Binggeli, Sandage & Tammann 1988). Current modeling of the conditional LF (CLF) to galaxy clusters in dark matter halos of a certain mass include the presence of central or brightest cluster galaxies (BCGs) with a log-normal CLF, while the rest of the galaxies (satellites) are given a power law CLF with a finite cut at high luminosities (Cooray & Milosavljevic 2005; Cooray 2006).

Special attention has always been paid to the high luminosity tail of the all galaxy LF. BCGs are the brightest of the old populations of red elliptical galaxies found in the high density cores of galaxy clusters are thought to have their progenitors formed at high redshift ($z \gtrsim 3$), and then have undergone a set of dry mergers in their life history (e.g. Ostriker & Hausman 1977; De Lucia & Blaizot 2007). Their importance lies in the low scatter of their luminosities, making them useful as standard candles (Postman & Lauer 1995; Loh & Strauss 2006; Lin et al. 2010; Paranjape & Sheth 2011; Dobos & Csabai 2011).

Several studies have been made to elucidate whether BCGs are the extremes of a red or early type galaxies LF or they come from other luminosity distribution. In order to answer the question, Geller & Tremaine (1976), Tremaine & Richstone (1977) and Bhavsar & Barrow (1985) investigated the statistics derived from the first and second brightest luminosities (and the gap between them) in galaxy clusters. Their results based on smaller samples has been confirmed by Loh & Strauss (2006), who found that the luminosity gap between first and second-ranked galaxies is substantially larger than what can be explained with an exponentially decaying luminosity function. On the other hand, Lin et al. (2010) shuffled the data to combine all galaxies of clusters to form a composite cluster, finding that BCGs in high luminosity clusters are not drawn from the luminosity distribution of all red cluster galaxies, while BCGs in less

[1] Department of Physics and Astronomy, Johns Hopkins University. 3400 North Charles Street, Baltimore, MD 21218, USA. e-mail: mtaghiza [at] pha.jhu.edu
[2] Institute for Theoretical Physics - HAS, Eötvös University, Pázmány sétány 1/a, 1117 Budapest, Hungary
[3] European Laboratory for Particle Physics (CERN), Geneva, Switzerland

luminous clusters are consistent to be the statistical extreme.

These previous studies were mainly directed toward the luminosity statistics within galaxy clusters. In this paper we will study galaxy luminosities as a whole, and the sampling will not be restricted to the maximal luminosities from galaxy clusters. This will keep the sample size large enough for studying the finite-size scaling behavior.

Since EVS is well known only for i.i.d. variables, one approach we will follow is trying to minimize the correlations between luminosities and positions by selecting the maximal luminosities from batches of galaxies in elongated regions or pencil beams along the line of sight, and defined by the footprint of the HEALPix tessellation on the sky (Górski et al. 2005). As we shall discuss, such elongated cells combined with the short range correlations in luminosities make possible an analysis of EVS based on the assumption that the luminosities approximate well an i.i.d. behavior. Another simple approach we will use for comparing with the previous method is the random sampling of the luminosity parent distribution in batches of fixed size. These are new approaches for testing the bright end of the overall LF, and inherently different from previous studies that considered testing the luminosity extremes in galaxy clusters.

Within the i.i.d. framework, the shape of the galaxy luminosity function is important for the EVS. The exponential tail in the high luminosity end of the LF would imply a Fisher-Tippett-Gumbel (FTG) EVS distribution, with corrections for the finite sample sizes depending on the power law at lower luminosities (Györgyi et al. 2008). In this analysis we will test the agreement with these expectations, and the analysis will also reveal whether or not a sharp cutoff at a high but finite luminosity exists.

We emphasize that even though the SDSS sample is large, the residual from the FTG distribution can be explained only when we consider the corrections due to both the finite size of the samples of each HEALPix pencil beam and the distribution present in the sample sizes (the number of galaxies in a cone is finite and varies from cone to cone). Thus we have here a pioneering example where a generalized finite size scaling (including sample-size distribution) is relevant in the data analysis.

The arguments and results will be presented in the following order. In Section 2 we describe our galaxy sample. Section 3 shows the fits to the galaxy luminosity distributions and functions, as well as details of the separation of the whole galaxy sample into blue and red samples according to cuts in a color-magnitude diagram. Section 4 explains the construction of the pencil beams and distribution of galaxy counts inside them. Section 5 contains a discussion of the basic concepts of extreme value statistics with emphasis on possible deviations from the expected limit distributions due to finite number of the galaxies in the pencil beams and, furthermore, due to the pencil-to-pencil fluctuations in the galaxy counts. In Section 6 we present the results about the distribution of maximal luminosities with the conclusion that within the uncertainties coming from the finiteness of samples and from the sample–size distribution, the Fisher–Tippett–Gumbel distribution gives an excellent fit. The final remarks and discussion can be found in Section 7.

Along this paper, we use the ($\Omega_{\rm L}$, $\Omega_{\rm M}$, h_0, w_0) = (0.7, 0.3, 0.7, -1) cosmology.

2. SAMPLE CREATION

In this paper we use photometric and spectroscopic data of galaxies from SDSS-DR8 (York et al. 2000; Stoughton et al. 2002; Aihara et al. 2011), available in a MS-SQL Server database that can be queried online via CasJobs [4], and analyzed directly inside the database using an integrated cosmological functions library (Taghizadeh-Popp 2010). The galaxies studied were the DR7 legacy spectroscopically-targeted Main Galaxy Sample (MGS) (Strauss et al. 2002), as well as the luminous red galaxies (LRGs) (Eisenstein et al. 2001). The sky footprint of the clean spectroscopic survey builds up from a complicated geometry defined by `sectors`, which cover a fractional area $F_A \simeq 0.1923$ of the whole sky. Redshift incompleteness arises from the fact that two 3" aperture spectroscopic fibers cannot be put together closer than 55" in the same plate. As a strategy, denser region in the sky are given a greater number of overlapping plates. However, only ∼93% (MGS) and ∼95% (LRG) of the initial galaxies photometrically targeted have their spectra taken.

Several selection cuts and flags were applied in order to have a clean sample. We selected only `science primary` objects classified as galaxies and appearing in calibrated images having the `photometric` status flag. We used the `score` quantity as a measure of the field quality with respect to the sky flux and the width of the point spread function, and selected only the fields in the range $0.6 \leq$ `score` ≤ 1.0. Furthermore, we neglected individual objects with bad deblending flags (`PEAKCENTER, DEBLEND_NOPEAK, NOTCHECKED`) and interpolation problems (`PSF_FLUX_INTERP, BAD_COUNTS_ERROR`) or suspicious detections (`SATURATED NOPROFILE`), as well with problems in the spectrum (`ZWARNING`) [5].

With respect to the MGS, they were observed as a magnitude limited sample, with a targeted r-band petrosian apparent magnitude cut of $m_r \leq 17.77$, and a redshift distribution peaking at $z \sim 0.1$. We further restrict this sample to safe cuts of $[m_{r,1}, m_{r,2}] = [13.5, 17.65]$. The lower limit is set due to the arising cross talk from close fibers in the spectrographs when they carry light from very bright galaxies, whereas the upper limit safely avoids the slight variations in the targeting algorithm of the limiting apparent magnitude around 17.77 over the sky. As shown in Fig. 1, we chose galaxies in the redshift interval $[z_1, z_2] = [0.065, 0.22]$, since at redshift lower than z_1, the galaxy high luminosity tail becomes incomplete (due to imposing the apparent magnitude cut at $m_{r,1}$). This left us with $N_g = 348975$ MGS galaxies in a volume of $V_{\rm S} = [V(z_2) - V(z_1)] \times F_A = 0.559{\rm Gpc}^3$. The full MGS sample will be further divided into a blue and red populations in Section 3.

With respect to the LRGs, they where selected from color cuts (in g-r v/s r-i space) in such a way that are traced across redshift as an old population of luminous and passively evolving red early type galaxies (Eisenstein et al. 2001). This was done by modeling them with an old stellar population spectral template from PEGASE (Fioc & Rocca-Volmerange 1997). We

[4] `http://casjobs.sdss.org`

[5] Detailed explanation in `sdss3.org/dr8/algorithms`

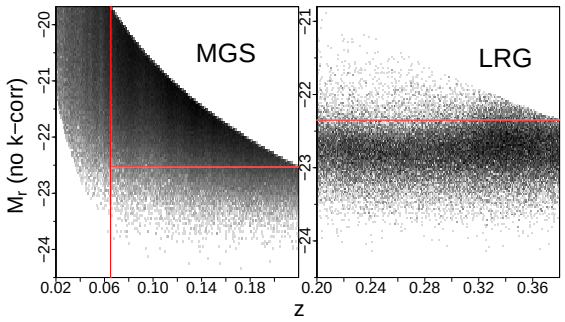

Figure 1. Completeness limits for the raw galaxy samples. Plotted are the petrosian absolute Magnitude v/s redshift histogram (log-scaled) for the full MGS and LRG samples. No k-correction nor evolution is applied at this point. The red horizontal lines show the absolute magnitude limits for a complete sample (-22.53 and -22.35 for MGS and LRG respectively). Note that for redshifts greater than z=0.065 (vertical red line), the MGS becomes complete at the bright end. This redshift limit was also checked using the Vmax method explained in Sec. 3.

use LRGs in the CUT I sample, which was built to be almost a volume limited sample up to redshift 0.38 with an r-band petrosian apparent magnitude cut of $m_{r,2} = 19.2$. We apply a safe redshift window of $[z_1, z_2] = [0.20, 0.38]$ since, at lower redshift, the color selection cuts admit blue galaxies belonging to the MGS. We further constraint this LRGs by considering galaxies whose r-band surface light profile can be modeled mainly as a DeVaucouleurs profiles (as in elliptical galaxies) more than an exponential disc (`fracDeV` ≥ 0.9) (Strateva et al. 2001). We also use the r-band concentration index R90/R50 (Shimasaku et al. 2001; Strateva et al. 2001) to select mostly elliptical galaxies (R90/R50$\geq$ 2.7). This left us with N_g =52579 LRGs in a volume of $V_S = 2.18\mathrm{Gpc}^3$.

Since our samples span broad redshift and time intervals, it is crucial to apply a (k+evolution)-correction to M_r in the form M_r = m_r - $DM(z)$ - $k(z)$ - $e(z)$, which brings all the galaxies to a common $z = 0$ rest-frame. The k-corrections for the MGS were calculated by modeling each galaxy spectrum as the closest non negative linear combination of spectra drawn from the Bruzual & Charlot (2003) templates (see Budavári et al. (2000) and Csabai et al. (2000)). We applied a simple average evolution correction as a linear function of redshift, derived by Blanton et al. (2003) as e(z)=-Qz (Q=1.62 for r-band, Q=4.22 for u-band). For the LRG case, we used the k+evolution correction derived from the PEGASE template. This was modeled as a 4th order polynomial in redshift, as used in Loh (2004) and Loh & Strauss (2006), where k(z)+e(z)=$0.115z$ +$5.59z^2$-$24.0z^3$+$36.0z^4$.

We finally checked the first 1000 images of galaxies for each sample ranked by brightest r-band petrosian absolute magnitude, and rejected the objects whose photometry appears to be ruined by the leaked light of a nearby star. Also, objects where rejected in the case when the petrosian magnitude was more different than 0.8 magnitudes compared with the model magnitude.

3. LUMINOSITY FUNCTIONS AND DISTRIBUTIONS

The luminosity function (LF), defined as the distribution of galaxy luminosities (or magnitudes) per volume, has been for long well studied as a basic statistic. Since galaxy surveys are generally apparent magnitude limited at the faint end, the LF differs from the luminosity distribution (LD) in that the former cannot be obtained from a simple raw histogram of the luminosity data points as LDs are. In fact, the faint luminosity tail of LDs is incomplete, as faint galaxies can be observed only at close enough distances (Malmquist bias). On the contrary, the brightest galaxies can generally be observed over the whole redshift limits of the survey. As a consequence, LFs are identical to LDs at the bright end (except for a scale factor equal to the survey's volume V_S) but start to depart from each other at a departure luminosity L_D (specified next).

The important link between LFs and LDs is that, since they behave the same way at the bright end, we can study LFs in this regime by instead doing the sampling and EVS on the LD of the individual data points. This is the strategy followed in this paper, which works as long as we sample galaxies with luminosities close enough to or brighter than L_D.

In order to correct the incompleteness of low luminosity galaxies, we construct LFs by adding more weight to these galaxies, as used in the Vmax method (Schmidt 1968), where each i-th galaxy is assigned a weight $w_i = V_S/V_{M,i} \geq 1$. Here we note that, given the particular $[z_1, z_2]$ and $[m_1, m_2]$ intervals for the survey, the i-th galaxy found at z_i could be observed only within a maximum comoving volume $V_{M,i}$ inside the overall volume V_S of the survey. If the i-th galaxy of apparent magnitude m_i, k-correction $k_i = k(z_i)$, evolution correction $e_i = e(z_i)$ and at a luminosity distance $D_L(z_i)$ were to have limiting apparent magnitudes $m_{1,2}$, then it should be moved to a limiting luminosity distance given by

$$D_{L,i}(z_{\rm lim}; m_{1,2}) = D_L(z_i) \times 10^{(m_{1,2}-k(z_{\rm lim})-e(z_{\rm lim})-m_i+k_i+e_i)/5}. \quad (1)$$

Hence, the maximum volume is defined by the biggest interval of D_L inside which a galaxy can appear in the survey:

$$V_{M,i} = [V(\min(D_L(z_2), D_{L,i}(z_{\rm lim}; m_2))) - V(\max(D_L(z_1), D_{L,i}(z_{\rm lim}; m_1)))] \times F_A, \quad (2)$$

As Eq. 1 defines $z_{\rm lim}$ in an implicit way, we solve for it iteratively. The weights $V_S/V_{M,i}$ are shown in Fig. 2. The departure magnitudes take the values of $M_D = -22.63$ (LRG) and $M_D = -22.43$ (MGS).

A non-parametric LF can be then easily estimated using a Vmax weighted histogram in the form

$$\Phi(M)\Delta M = \frac{1}{\Delta M} \sum_{M_i \in \Delta M} \frac{c_i}{V_{M,i}}, \quad (3)$$

The extra weight c_i takes into account the incompleteness of the target selection algorithm for spectroscopic follow up. The error $\delta\Phi(M_r)$ is estimated by using Jack-Knife sampling of 38 regions about 200 SqDeg each.

Since MGS (hereafter MGSall) galaxies can be classified into roughly a blue (MGSblue) and red (MGSred) populations, we do EVS on these 2 classes separately, as the bright end of the MGSall is dominated by the red component. For this, we construct a color-magnitude diagram (CMD) using the Vmax weighting, and create a separating curve between the 2 classes, just as done by Baldry et al. (2004).

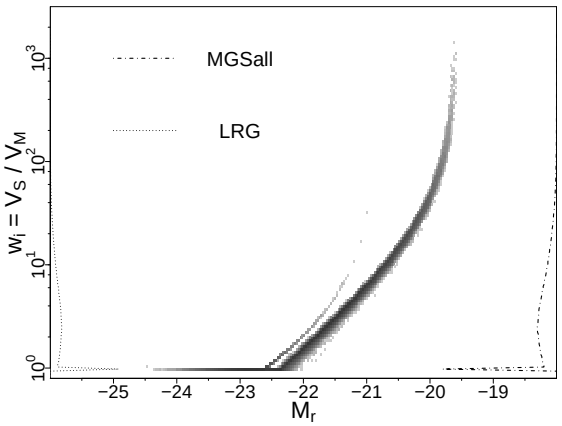

Figure 2. 2-Dimensional histogram (in logarithmic gray-scale) showing the onset of absolute magnitude incompleteness. For the LRGs (left branch), we see $w_i \geq 1$ and $w_i \geq 2$ starting at $M_r = -22.63$ and $M_r = -22.05$). For MGSall (right branch), it happens at $M_r = -22.43$ and -21.91, respectively. The curves against the vertical axis are the corresponding (unnormalized) distributions of the weights w_i.

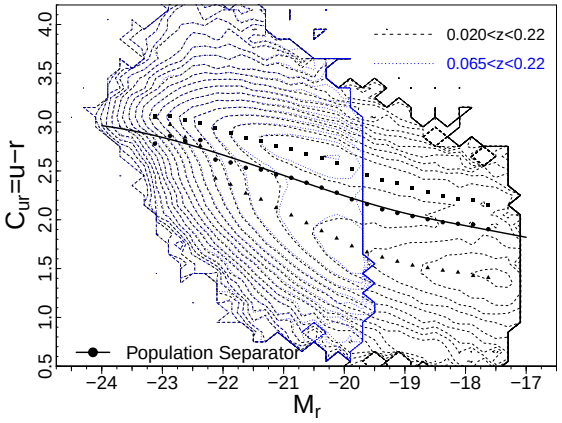

Figure 3. Color magnitude diagrams of the MGSall sample ($0.065 < z < 0.22$), compared to the one of the full MGS in the range $0.02 < z < 0.22$. Bin size is $\{\Delta C_{ur}, \Delta M_r\} = \{0.1, 0.2\}$. The log-scaled height contour curves are spaced in $\Delta \log_{10}(\text{height}) = 0.25$, starting at height=1. The triangles and squares indicate the fitted values of the Bimodal Gaussian μ parameter for the blue and red populations, respectively. The solid thick line is the population separator in Eq.6 fitted to the filled circles, which trace the separating level curve.

The CMD of MGSall is shown in Fig. 3, where the color $C_{ur} \equiv u - r$ is calculated using model magnitudes. There is a smooth separation between the MGSblue and MGSred classes, whose joint distribution resembles a bimodal Gaussian in color space at each magnitude bin. Following Baldry et al. (2004), we fit the CMD to

$$\Phi(M_r, C_{ur}) = \Phi_B(M_r, C_{ur}) + \Phi_R(M_r, C_{ur}) \quad (4)$$
$$\Phi_{B;R}(M_r) = \phi_{B;R} N(C_{ur}; \sigma_{B;R}(M_r), \mu_{B;R}(M_r))$$

where $N(C_{ur}; \sigma, \mu)$ is a normal gaussian distribution and $\phi_{B;R}(M_r)$ are the amplitudes, proportional to the respective luminosity functions of the MGSblue or MGSred populations.

We further construct a color-separating curve $C_S(M_r)$ between the classes *Red* and *Blue* using a gaussian classifier in the context of Bayes theorem. At each magnitude bin centered at M_r we equate the posterior probabilities, finding the color $C_S(M_r)$ that satisfies $P(Blue|C_S(M_r)) = P(Red|C_S(M_r))$. In this way, the separating curve is defined such that on top of it the galaxies have the same probability of belonging to either classes. Since $P(Red; Blue) = \phi_{R;B}/(\phi_B + \phi_R)$, we have at each M_r

$$P(C_S|Blue)P(Blue) = P(C_S|Red)P(Red)$$
$$\Phi_B(M_r, C_S) = \Phi_R(M_r, C_S). \quad (5)$$

The curve C_S defines the contour where the individual distributions of each class touch each other. Since MGSall does not reach fainter magnitudes than $M_r \simeq -19.6$, we extend it to z=0.02 in order to get a good view and fit of C_S at the low luminosity tail. For the fitting, we follow (Baldry et al. 2004) and parametrize the separating curve (shown in Fig. 3) as

$$C_S(M_r) = p_0 + p_1(M_r + 20) + p_2 \tanh\left[(M_r - p_3)/p_4\right], \quad (6)$$

where we found (p_0,p_1,p_2,p_3,p_4)=(2.275,-0.071,-0.20,-20.23,1.30), as shown in Fig. 3. The separator leads to $N_g = 134575$ and $N_g = 214400$ galaxies in the MGSblue and MGSred samples respectively, considering the range $M_r \leq -20.2$.

The luminosity functions and distributions and their fits are shown in Fig. 4, and Tables 1 and 2 contain the fitting parameters.

For the MGS samples, we use a generalized gamma as a fitting function, which results in the known Schechter profile (Schechter 1976) when $\beta = 1$:

$$\Phi(L)dL = \Phi_* \left(L/L_*\right)^{\alpha} \exp\{-\left[(L/L_*)^{\beta}\right]\}dL. \quad (7)$$

The normalization factor Φ_* is left as a free parameter for LFs, whereas for the LDs is defined by $\Phi_* = \beta/[L_*\Gamma((\alpha+1)/\beta, L_{\min})]$, where the incomplete gamma function $\Gamma(*, L_{\min})$ is the integral in the interval $[L_{\min}, \infty]$. The fitted luminosity values for the LFs and LDs we converted into magnitude units using M_r=$-2.5\log_{10}[L/L_\odot]+M_{\odot,r}$, where $M_{\odot,r} = 4.62$ (Blanton et al. 2001) and $L_\odot$ is the solar luminosity in the r band. Note that the MGSred LF reaches brighter magnitudes than the MGSblue sample, and its high luminosity tail can be better fitted using the generalized gamma function compared with the more common Schechter fit. On the other hand, the Schechter fit is well suited for the MGSblue LF. Note the higher fraction of blue galaxies at fainter magnitudes, as demonstrated by the stronger faint end slope α in the Schechter fit.

The LRG sample was made to include the brightest early types. Therefore, they are naturally better fitted with an extreme value distribution (EVD) or its special case the Gumbel where $\xi = 0$ (see Sec. 5):

$$\Phi(L) = \Phi_* \text{EVD}(L), \quad (8)$$
$$\text{EVD}(L) = L_\sigma^{-1} t(L)^{\xi+1} \exp(-t(L))dL, \quad (9)$$
$$t(L) = (1 + \xi[\tfrac{L-L_\mu}{L_\sigma}])^{-1/\xi}, 1 + \xi[\tfrac{L-L_\mu}{L_\sigma}] > 0.$$

with L_μ, L_σ and ξ being respectively the location, scale and shape (or tail index) fitting parameters. The LRGs were built to be a complete (volume limited) sample, but some scattered lower luminosity galaxies passed the color

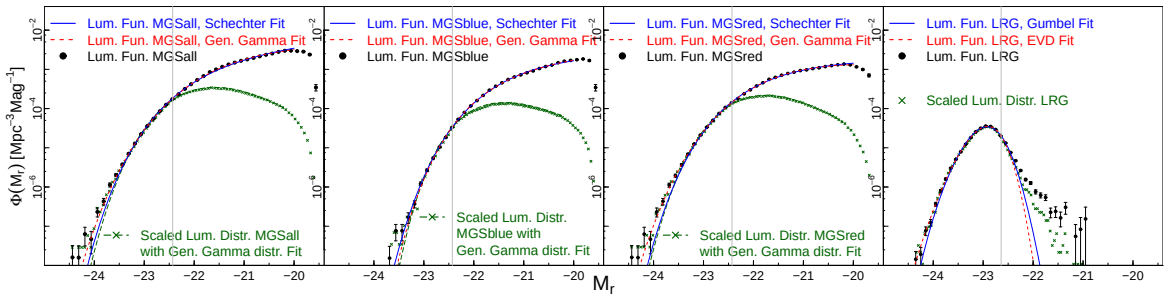

Figure 4. Luminosity functions and distributions of the different galaxy samples, together with the best Schechter, generalized gamma, Gumbel and EVD fits from Tables 1 and 2. The vertical lines denote the completeness boundary $w_i = 1$, where the LFs depart from LDs. The LDs were scaled by the factor N_g/V_S in order to compare them with the LFs.

Table 1
Luminosity Function Fitting parameters.[a]

Sample	Φ_* [10^{-3} Mpc^{-3}Mag^{-1}]	M_*	α	β
	Schechter	Fitting		
MGSall	3.10 ± 0.05	-21.46 ± 0.02	-1.34 ± 0.04	1
MGSblue	2.70 ± 0.05	-20.87 ± 0.02	-1.06 ± 0.03	1
MGSred	2.06 ± 0.05	-21.41 ± 0.02	-0.99 ± 0.03	1
	General	Gamma	Fitting	
MGSall	7.79 ± 0.38	-20.42 ± 0.10	-0.81 ± 0.05	0.75 ± 0.02
MGSblue	1.79 ± 0.26	-21.22 ± 0.10	-1.28 ± 0.08	1.14 ± 0.05
MGSred	3.71 ± 0.11	-20.33 ± 0.17	-0.48 ± 0.08	0.74 ± 0.03
Sample	Φ_* [10^{-5} Mpc^{-3}]	M_μ	M_σ	ξ
	Gumbel	Fitting		
LRG	2.52±0.03	-22.85±0.01	-21.36±0.02	0
	GEV	Fitting		
LRG	2.49±0.02	-22.86±0.01	-21.36±0.02	0.04±0.01

[a] Parameters from fitting to Eq. 7 (MGS) or Eq. 8 (LRG). Parameters in luminosity units (L_*, L_μ and L_σ) were converted into absolute magnitudes (M_*, M_μ and M_σ) using $M{=}{-}2.5\log_{10}[L/L_\odot]{+}M_\odot$, where $M_\odot = 4.62$, everything measured in the petrosian r-band. MGS and LRG samples are fitted in the ranges $M_r \leq -20.2$ and $M_r \leq -22.64$ respectively.

Table 2
Luminosity Distribution Fitting parameters.[a]

Sample	M_*	α	β
	General	Gamma	Fitting
MGSall	-19.99 ± 0.16	1.52 ± 0.10	0.79 ± 0.03
MGSblue	-21.02 ± 0.11	0.72 ± 0.10	1.18 ± 0.05
MGSred	-20.18 ± 0.16	1.67 ± 0.11	0.82 ± 0.03

[a] Parameters from fitting to Eq. 7 (MGS) using $\Phi_* = \beta/(L_*\Gamma((\alpha+1)/\beta, L_{\rm min})$. We used $M_{\rm max} \equiv M(L_{\rm min}) = -20.2$. Parameters in luminosity units were converted into absolute magnitudes.

cuts and contaminated it (Fig. 1). Therefore, we only fit the LF up to the completeness limit $M_{\rm D} = -22.64$ as explained earlier.

4. SAMPLING THE MAXIMAL LUMINOSITIES: CREATION OF I.I.D. BATCHES AND HEALPIX-BASED PENCIL BEAMS

Classic extreme value statistics needs close-to-i.i.d realizations of the underlying parent probability distribution from which to draw the maximal values.

A common practice in EVS is using the block maxima approach, where the data is grouped in consecutive blocks or batches. This creates n batches, with all the batches having the same number N of data points (batch size). This is the first approach that we follow in this paper, where the batches are chosen by random sampling without replacement.

In some real life situations, such as time series, the blocks are chosen to span each of the many different cycles of the underlying process (e.g. years, days or usage cycles). Of course, some blocks might present missing or sparse data, due to bad sampling strategies or sensor failures. In other cases, time series or spatial data are correlated and clump in clusters of different sizes that exceed a certain threshold level (e.g., insurance claims after a hurricane). In all these situations, the different realizations of the parent probability distribution will have different number N of data points, with distribution P(N).

In order to extend and study EVS under the extra influence of a P(N), we decided to use a second sampling approach. We recreate this situation by dividing the sky in equal-area spherical patches, each one defined by an individual cell of the HEALPix tessellation (Górski et al. 2005). This creates 1-dimensional pencil-like beams, each of which containing one close-to-i.i.d realization of the galaxy distribution through redshift and with a variable galaxy number N. Note that this method is essentially different to sampling maximal luminosities from galaxy clusters, as these are highly correlated. We start with a finer SDSS DR8 spectroscopic footprint with resolution $N_{side} = 512$ (of cell size $\sqrt{\Omega_{pix}} \simeq 6.87'$).

We further degrade the footprint into 3 lower resolution maps defined by $N_{side} = 16, 32$ and 64, creating thus the cells that define the pencil beams. Note that these bigger cells may partly cover an area not belonging to the footprint. Hence, we define the fractional area occupancy f as the area inside the footprint covered by the cell divided by the total area of the cell. The cumulative distribution of f (Fig. 5) shows clear breakpoints at $f \sim 0.97$ for all 3 resolutions. We therefore decide to use only the group of cells which satisfy $f \geq 0.97$. A summary on the 3 different resolution HEALPix schemas is presented in Table 3, and HEALPix maximal luminosity maps are shown for MGSall in Fig. 6.

4.1. *Distributions of galaxy counts in a HEALPix cell*

The number of galaxies N fluctuates in the pencil beams. Unless the galaxy-count distribution in a HEALPix cell $\mathcal{F}(N)$ is very narrow, this affects the limit distribution one expects for the extreme luminosities. We have thus evaluated $\mathcal{F}(N)$ for the MGS and LRG sam-

Table 3
HEALPix schemas for the different galaxy samples [a]

HEALPix schemas										
N_{side}	$\sqrt{\Omega_{pix}}$	n_{sphere}	n_F MGSall	n_F MGSblue	n_F MGSred	n_F LRG	$n_{F,97}$ MGSall	$n_{F,97}$ MGSblue	$n_{F,97}$ MGSred	$n_{F,97}$ LRG
16	3.66^o	3072	768	767	767	755	473	473	473	473
32	1.83^o	12288	2659	2644	2653	2591	2030	2030	2030	2029
64	$55.0'$	49152	10017	9937	9991	9461	8492	8489	8490	8256

[a] Here, n_{sphere} is the total number of HEALPix cells in the sky (each of area Ω_{pix}), n_F is the number of galaxy-containing cells inside the footprint and $n_{F,97}$ is the number of cells with areas included at least 97% inside the footprint.

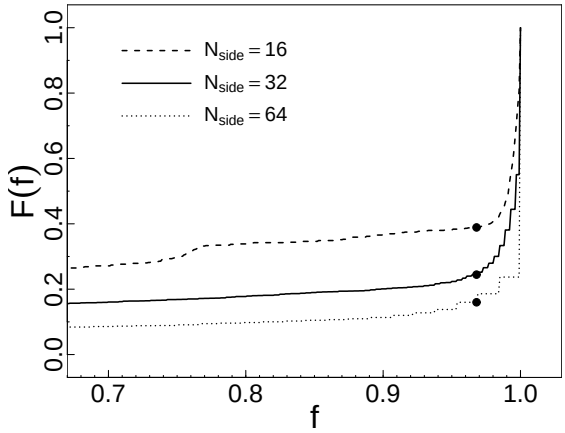

Figure 5. Cumulative distribution of the HEALPix cell fractional occupation area f, shown for the 3 different footprint cell sizes. The black filled dots show the breakpoints at $f = 0.97$. We consider only cells with $f \geq 0.97$

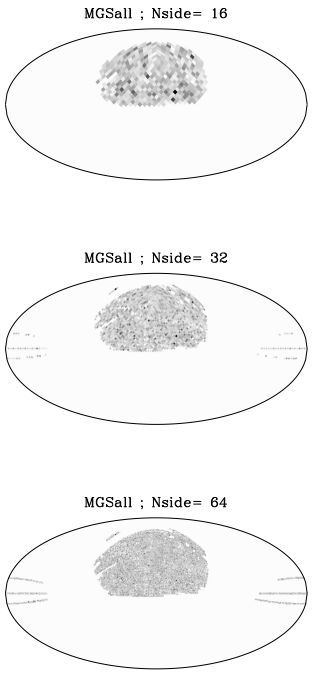

Figure 6. HEALPix Maps of maximal luminosities (in linear scale) for the MGSall galaxy sample at different values of N_{side}. Darker color means higher luminosity. Only cells included 97% in the footprint are shown. The SDSS-DR8 footprint boundaries become evident at resolution $N_{side} = 64$.

ples, and the results for decreasing N_{side}, i.e. for increasing average of the galaxy count $\langle N \rangle$ are shown in Fig.7.

As one can see, the $N_{side} = 64$ suggest good statistics yielding smooth functions. We should note, however, that the average galaxy count is rather low in this case ($\langle N \rangle \approx 5 - 40$), so it is far from the limit $\langle N \rangle \to \infty$ one would like to take when investigating the EVS.

There are two lessons to learn from Fig.7. First, the distributions are rather narrow which suggests that it is a reasonable assumption that the theory of EVS known for fixed N can be applied to galaxy luminosity. Second, one can develop analytic approximations to these histograms. Indeed, the distributions can be relatively well approximated by a gamma function with free location and scale parameters.

5. THEORY OF EXTREME VALUE STATISTICS

5.1. *Classical Theory*

Extreme value statistics (EVS) is concerned with the probability, $P_N(v)dv$, of the largest value in a batch of N measurements $\{v_1, v_2, ..., v_N\}$ being $v = \max_i v_i$. For us, the v_is are galaxy luminosities, obtained by either random sampling N galaxies from the sky, or chosen from the HEALPix cells covering the sky, each with a variable N.

The results of the EVS are simple provided the v_is are i.i.d. variables drawn from a general parent distribution $f(v_i)$. Namely, the limit distribution $P_{N\to\infty}(v)$ belongs to one of three types and the determining factor is the large-argument tail of the parent distribution (Gumbel 1958; Galambos 1978). Frechet type distribution emerges if f decays as a power law, Fisher-Tippett-Gumbel (FTG) distribution is generated by fs which decays faster than any power law and, finally, parent distributions with finite cutoff and power law behavior around the cutoff yield the Weibull distribution (Gumbel 1958; Galambos 1978). All the above cases can be unified as a generalized EVD whose integrated distribution $F_N(v)$ is given in the $N \to \infty$ limit by

$$F(v) = \exp\left\{-\left[1 + \xi\left(\frac{v-\mu}{s}\right)\right]^{-1/\xi}\right\} \qquad (10)$$

with parameters μ, s and ξ. The shape parameter ξ can take values $\xi > 0, = 0, < 0$, which correspond to the Frechet, FTG, Weibull classes, respectively. The parameter ξ is also called the tail index, since it is related to the exponent of the large-argument power-law behavior. The probability density function associated to Eq. (10) is shown in Eq. (9).

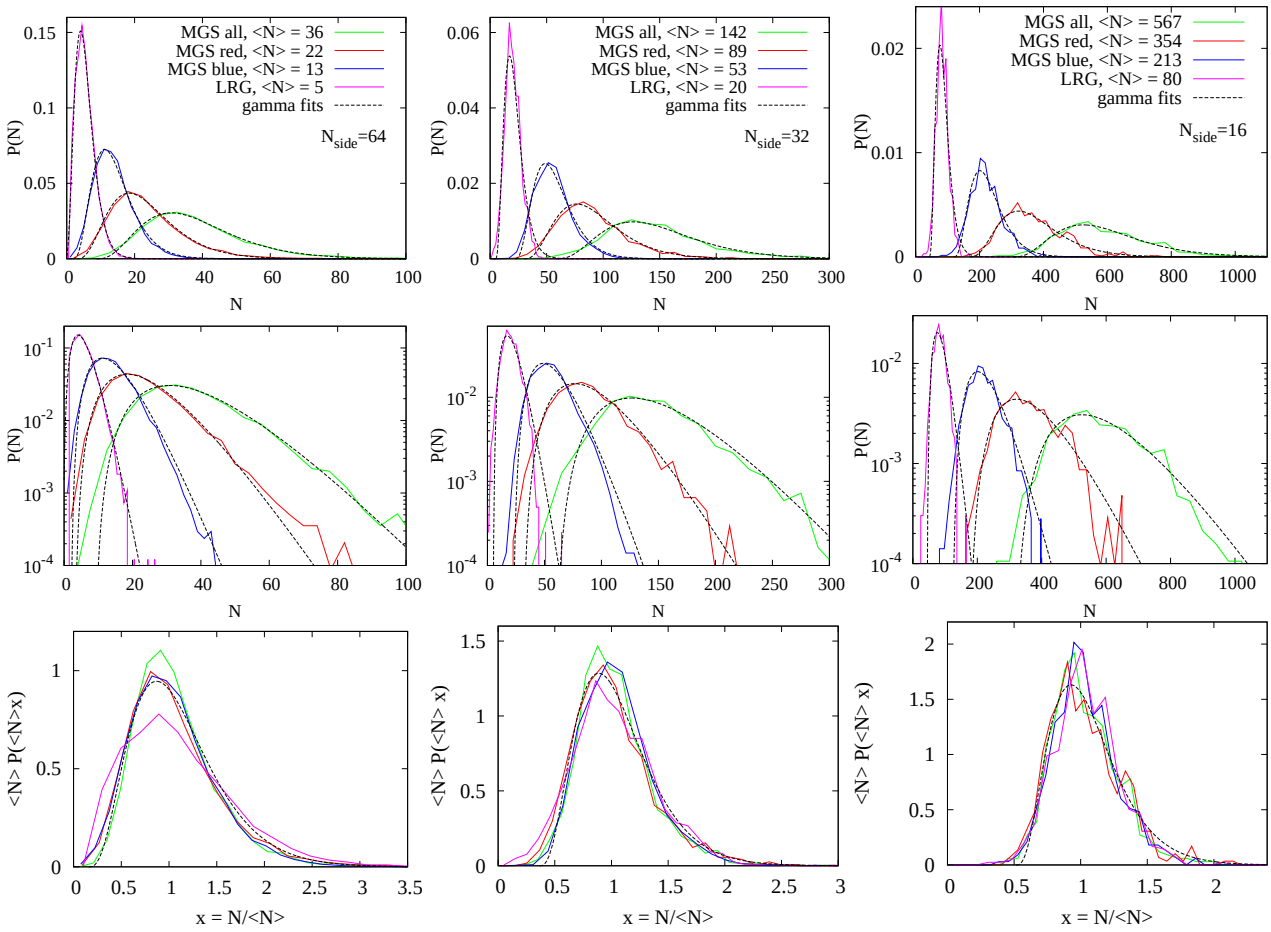

Figure 7. Galaxy count distributions in a HEALPix cell of size $N_{side} = 64$, 32, and 16, i.e. for increasing average galaxy count $\langle N\rangle$. Gamma function of the form $\mathcal{F}(N) \sim (N/\overline{N} - d)^3 \exp(-N/\overline{N} + d)$ fits well the distributions as can be seen on linear (first row) and semilog scale (second row). Count distributions for different galaxy samples can be scaled together by the average number of galaxies in a cell $\langle N\rangle$ (third row).

The EVS has been developed mainly for i.i.d. variables and there are only a few well established results for systems with correlations between the v_is. These results are mainly related to sufficiently weakly correlated variables where the i.i.d. results can be shown to apply (Bermann 1964; Györgyi et al. 2007). In the following we shall assume that the correlations between the galaxy luminosities are sufficiently weak so that the experimental histograms can be compared with the i.i.d. results. This assumption is important for the sampling in HEALPix cells in the sky, but not in a random sampling schema (arguments in favor of this assumption will be discussed in Section 7 using the knowledge of the correlations between galaxy positions).

The parent distribution for galaxy luminosities is known to be well fitted by the Gamma-Schechter distribution $\Phi(L) = \Phi_*(L/L_*)^\alpha \exp[-(L/L_*)^\beta]$ as given in (7) where L^* sets the scale, and $\alpha \approx -1$ together with $\beta = 1$ is the Schechter profile. For this parent distribution, the theory of EVS tells us that the limit distribution of extremal luminosities belongs to the FTG class ($\xi \to 0$)

$$P(v) = \frac{dF(v)}{dv} = a \exp\left[-(av+b) - e^{-(av+b)}\right] . \quad (11)$$

where the parameters can be fixed by setting $\langle v\rangle = 0$ and $\sigma = \sqrt{\langle v^2\rangle - \langle v\rangle^2} = 1$, yielding $a = \pi/\sqrt{6}$ and $b = \gamma_E \approx 0.577$. It should be emphasized that this choice leads to a parameter-free comparison with the empirical data. In fact, the histogram of the maximal luminosities $P(v)$ should be plotted in terms of the variable $x = (v - \langle v\rangle_N)/\sigma_N$ where $\langle v\rangle_N$ is the average of the maximal luminosity while $\sigma_N = \sqrt{\langle v^2\rangle_N - \langle v\rangle_N^2}$ is its standard deviation. The resulting scaling function should approach the universal function (11) in the $N \to \infty$ limit

$$P_N(x) = \sigma_N P_N(\sigma_N x + \langle v\rangle_N) \to P(x) . \quad (12)$$

5.2. *Deviations from the Classical Theory*

In addition to the assumption of v_is being i.i.d. variables, there are two additional problems with the program of comparing the data with the theory. First, a notorious aspect of EVS is the slow convergence of $P_N(x)$ to the limit distribution $P(x)$. Second, the batch size N (the number of galaxies in a given solid angle) varies with the direction of the angle. Thus the histogram of the maximal luminosities $P_N(x)$ is built from a distribution of Ns. Both of the above effects introduce corrections to the limit distribution we are trying to use for comparison. Below we estimate the magnitude of these corrections.

5.2.1. *Finite size corrections*

Finite size corrections in EVS have been studied in detail with the main conclusion that to first order in the vanishing correction in the $N \to \infty$ limit, the scaling function can be written as

$$P_N(x) \approx P(x) + q(N)P_1(x)\,, \tag{13}$$

where $q(N \to \infty) \to 0$ and the shape correction $P_1(x)$ is universal function. Both the amplitude q and the shape correction $P_1(x)$ are known for Schechter type parent distributions. The convergence to the limit distribution is slow since we have (Györgyi et al. 2008, 2010)

$$q(N) = -\frac{\alpha}{\ln^2 N}\,. \tag{14}$$

for $\beta = 1$. In the general case of a parent following the generalized gamma distribution of Eq. (7), with $\beta \approx 1$, there are two terms which may have comparable contributions (with the shape correction function being identical)

$$q(N) = \frac{(1-\beta)}{\beta \ln N} + \frac{(2\beta-1)(\beta-\alpha-1)}{\beta^2 \ln^2 N}. \tag{15}$$

Note that this theoretical construct needs the values of α and β to be fitted at the bright end tail of the luminosity distribution, thus neglecting the low luminosity tail (Györgyi et al. 2010). The value of β is roughly 1, thus for a characteristic range of $N \approx 10-200$, the amplitude is of the order of 0.2-0.04. Thus one can expect a 20-4% deviations coming from finite-size effects.

The finite-size shape correction is also known (Györgyi et al. 2008):

$$P_1(x) = \left[P(x)\left[-\frac{ax^2}{2} + \frac{\zeta(3)x}{a^2} + \frac{a}{2}\right]\right]' \tag{16}$$

where $a = \pi/\sqrt{6}$ and $\zeta(z)$ is the Riemann zeta function. The function $P_1(x)$ is plotted on Fig.8 and one can see that the first order correction has well defined signs in various regions of x.

A special case arises when the parent distribution is of Gumbel type. In this case, the EVD is also a Gumbel, but with no apparent finite size correction. This is due to the fact that the Gumbel distribution is a fixed point in the renormalization theory formalism used for obtaining the first order corrections (Györgyi et al. 2008, 2010). As a result, the deviations should be caused only by random shot noise from the data points.

5.2.2. *Variable batch size*

Variable sample size raises basic questions about EVS. In particular, the limiting procedure of sample size going to infinity becomes a problem. If the normalized distribution of N is known $\mathcal{F}(N)$ then it is natural to consider the average $\overline{N} = \int \mathcal{F}(N) N dN$ as the parameter corresponding to the fixed sample size of the usual EVS. Therefore, using the limit $\overline{N} \to \infty$, the extreme value distribution becomes

$$\overline{P}(v) = \lim_{\overline{N}\to\infty} \int_0^\infty \mathcal{F}(N) P_N(v) dN\,. \tag{17}$$

Once $\overline{P}(v)$ is known, we can write it in scaled variables thus obtaining $\overline{P}(x)$ and the difference $\overline{P}_1(x) \equiv P(x) - \overline{P}(x)$ provides us an estimate of corrections coming from the variable sample size.

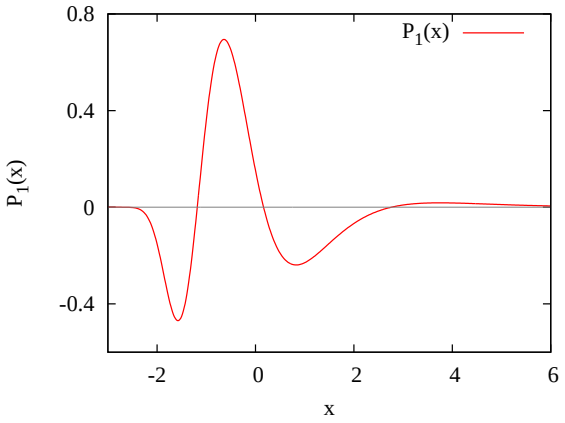

Figure 8. First order finite size shape correction function in finite-size scaling of EVS with the Schechter function being the parent distribution. The amplitude of this correction is of the order of $1/\ln N$ for $\beta \neq 1$ while it is of the order of $1/\ln^2 N$ if $\beta = 1$.

The actual calculation of $\overline{P}(x)$ assumes that we know $\mathcal{F}(N)$. A simple form of $\mathcal{F}(N)$ which fits the observed distribution reasonably well (see Fig.7) and allows analytic calculations is given by

$$\mathcal{F}(N) = \frac{(N/\overline{N} - d)^k}{\overline{N}\Gamma(k+1)} \exp(-N/\overline{N} + d), \tag{18}$$

where $k = 3$ and d is a free parameter distinct from zero, since there is a finite cut in N ($N > N_0 = \overline{N}$). Note that here we assumed that the distribution can be written in a scaled form

$$\mathcal{F}(N) = f(N\,/\,\overline{N})/\,\overline{N}\,. \tag{19}$$

This is a good approximation to all of the experimental distributions. Using the above $\mathcal{F}(N)$, one finds that the limit distribution is universal within the FTG class (and so, for the Schechter function parent distribution as well)

$$\overline{P}(v) = \frac{[k+1+d(1+e^{-v})]\exp(-de^{-v}-v)}{[1+e^{-v}]^{k+2}}. \tag{20}$$

The appropriately scaled distribution (x variable) for the case of $d = 0$ and $k = 3$ is given by the following expression

$$\overline{P}(x) = \frac{4a\exp(-ax-b)}{(1+\exp(-ax-b))^5}\,, \tag{21}$$

where $a = \sqrt{\frac{\pi^2}{3} - \frac{49}{36}}$ and $b = \frac{11}{6}$.

The functions $\overline{P}(x)$ and $P(x)$ (FTG), and their difference is displayed on Fig.9. We can see that the maximal difference $\overline{P}_1(x) = \overline{P}(x) - P(x)$ is of the order of 10%. What is more interesting is that the positive and negative regions of the differences are significantly shifted compared to those of the finite size corrections (Fig.8). Thus the two correction may amplify as well as cancel each other, depending on the parent distribution and on $\mathcal{F}(N)$.

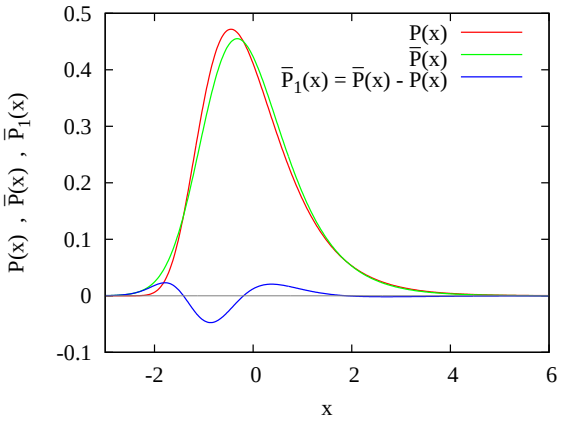

Figure 9. Comparison of the FTG limit distribution (red) with that obtained from the variable sample size case with the sample-size distribution given by Eq.(18) (green line, for the case of $d = 0$ and $k = 3$). The difference of the two functions is also shown, being in the order of 10%.

6. DISTRIBUTION OF MAXIMAL LUMINOSITIES AND THE EMPIRICAL FIRST ORDER CORRECTIONS

In order to compute statistics on the maximal luminosities, we used the 2 sampling methods (random sampling and HEALPix-based batches) explained in section 4. As we deal with a fixed number N_g of galaxies, there is a bias-variance trade-off in all statistics calculated. In fact, increasing the number of batches n does indeed decrease the variance. However, at the same time the data points per batch N decreases, which departs us from the ideal case of $N \to \infty$, having an increase in the bias. All the statistics are then subject to the balance between N and n.

One interesting statistic we measured empirically is the tail index ξ on the extreme value distribution in Eq. (9), which is the probability density distribution associated to Eq. (10). The importance of ξ is that it specifies whether the parent distribution has an infinite reaching tail ($\xi \geq 0$) or a finite cut ($\xi < 0$) at a certain maximum luminosity. Next, we measured as well the first order finite size correction for the random sampling method, as well as the influence of the variable batch size in the HEALPix-based method.

6.1. *Statistics from random sampling batches*

6.1.1. *The Tail index ξ*

The tail index ξ can be readily calculated in standard EVS using the maximum likelihood estimator on Eq. (9). We tried this for various combinations of n and N. The fitted parameters are in Table 4, with probability distributions of the maximal luminosities (in magnitude-space) shown in Fig. 10. Note that the maximal luminosities are mostly sampled in the region where $w_i \leq 2$, which assure us that we are sampling also from the luminosity function. Note the good overall fit to the EVDs, as well as the increase of L_μ as N increases. The value of L_μ for the LRGs is about twice the size of that for the MGSall. As the amount n of batches decreases with N, the dispersion and errors in the parameters also increase at higher N as expected.

For the MGS samples, the value of ξ seems to be positive but very close to zero, with $\xi < 0$ being unlikely to happen. Note that for both MGSall and MGSred, the tail index decreases with increasing N, so the deviation

Table 4
Fitting parameters for maximal luminosities[a]

Sample	N	n	L_μ $[10^{10} L_\odot]$	L_σ $[10^{10} L_\odot]$	ξ
MGSall	24	14540	7.99 ± 0.03	1.98 ± 0.03	0.086 ± 0.011
(N_g=348975)	50	6979	9.48 ± 0.05	2.10 ± 0.04	0.091 ± 0.017
	100	3489	10.96 ± 0.08	2.26 ± 0.06	0.089 ± 0.023
	200	1744	12.59 ± 0.12	2.43 ± 0.09	0.079 ± 0.033
MGSblue	24	5607	6.07 ± 0.04	1.30 ± 0.03	0.012 ± 0.016
(N_g=134575)	50	2691	7.01 ± 0.05	1.29 ± 0.04	0.038 ± 0.024
	100	1345	7.88 ± 0.07	1.30 ± 0.06	0.054 ± 0.036
	200	672	8.82 ± 0.11	1.32 ± 0.08	0.068 ± 0.051
MGSred	24	8933	8.81 ± 0.05	2.14 ± 0.04	0.080 ± 0.015
(N_g=214400)	50	4288	10.46 ± 0.07	2.25 ± 0.05	0.081 ± 0.021
	100	2144	12.09 ± 0.11	2.40 ± 0.08	0.070 ± 0.029
	200	1072	13.82 ± 0.16	2.56 ± 0.12	0.060 ± 0.038
LRG	24	2190	17.91 ± 0.12	2.72 ± 0.09	0.002 ± 0.028
(N_g=52579)	50	1051	19.86 ± 0.18	2.81 ± 0.13	-0.016 ± 0.038
	100	525	21.75 ± 0.26	2.80 ± 0.18	-0.008 ± 0.054
	200	262	23.69 ± 0.36	2.77 ± 0.25	-0.010 ± 0.075

[a] Parameters from the maximum likelihood fitting of the extreme value distribution in Eq. 9. Maximal luminosity values are sampled at n batches of fixed size N. Quoted are the 1-σ standard errors. N_g denotes the total number of galaxies in each sample.

of ξ from zero may be just a finite size effect. In fact, we can observe that $\xi \sim q(N)$, which is actually the theoretical prediction if we assume a FTG EVD (Györgyi et al. 2010). For the MGSblue, the tail index increases with N, but the error is roughly equal to ξ itself, and also increases. The case of the LRG is quite clear, where the value of the tail index does not have a dependence on N, having $\xi \approx 0$ within the errors.

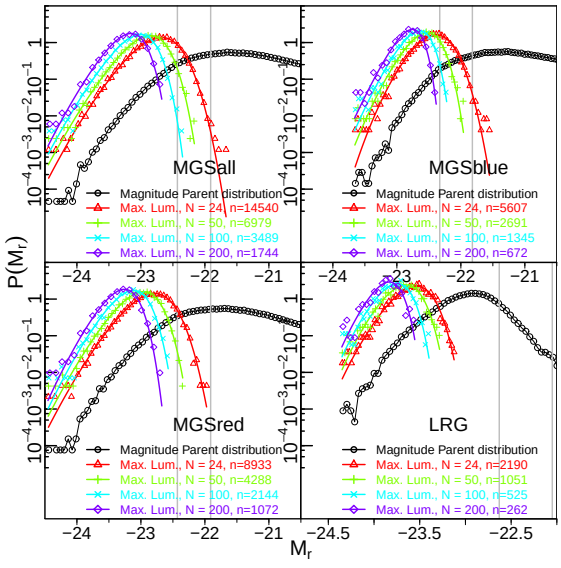

Figure 10. Distribution of r-band absolute magnitude M_r of the full samples. Also included are the distribution of the maximal luminosity for each sample according to the fixed batch size sampling. The vertical lines show the points where $w_i = 1$ (left line) and $w_i = 2$ (right line).

6.1.2. *The First order Finite Size Correction*

Motivated by the presence of a finite-N, we analyzed the behavior of the empirical finite size corrections for the EVD, and plotted them in Fig. 11. Since the estimated values of ξ in the previous section are zero or a small positive number, which is difficult to specify precisely, we assumed for simplicity $\xi = 0$ and used the theoretical corrections in 5.2.1 (theoretical corrections for $\xi \neq 0$ are not developed yet). Here, the empirical corrections are obtained by standardizing the maximal luminosities and subtracting them from the standard Gumbel distribution. For plotting the theoretical corrections with an amplitude given in Eq. (15), we need appropriate values of α and β. As explained in Sec. 5.2.1, these fitting parameters should come from fitting the high luminosity tail. Therefore, the fitted values of the full LD in Table 2 should not be used. In our case, Fig. 4 shows that the full luminosity function fit (Table 1) is a much better approximation of the high luminosity tail, and we use it instead.

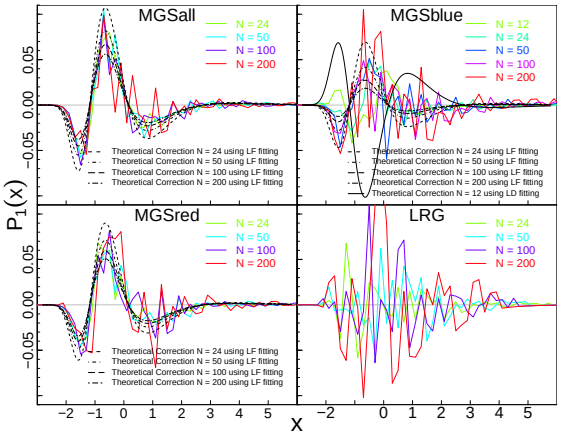

Figure 11. Empirical finite size corrections from n batches of fixed size N (from Table 4). Each simulation is made by random sampling (without replacement) of a fixed number N of luminosity data points. Also, the theoretical first order correction in Eq. 13 is shown for the cases N=24,50,100,200 (with decreasing amplitude).

Fig. 11 shows that the empirical corrections for MGS galaxies do have the same shape than the theoretical first order correction. The amplitude of the function approximately agrees, but we found that the empirical amplitude does not increase significantly when N decreases. On the contrary, it seems to decrease especially in the MGSblue case where it changes its sign as well. The explanation is that as N becomes smaller, we start sampling the maximal luminosities from the bulk of the luminosity distribution instead of its high luminosity tail. Of course, the departure of LF and LD in this regime makes the LF fitting parameters α and β no longer valid for calculating the theoretical corrections. Moreover, small N might require adding the next term in the correction. These considerations might explain the fact that the empirical corrections can change sign when N becomes small, as seen in the $N = 12$ case for the MGSblue. In this case, we tried the α and β parameters obtained by fitting the luminosity full distribution (Table 2), since they are of course a much better fit of the low luminosity tail of the LD than the ones from the LF fitting. As a result, the theoretical correction now has the same sign as the empirical correction, although a different amplitude. A compromise can be reached by fitting the LD not to the full extend of the faint end, but to intermediate values of luminosities.

In the LRG case, we cannot find a systematic correction, but just noise. This is in agreement with the expected behavior as explained in Sec. 5.2.1, since the Gumbel parent distribution is a fixed point in the renormalization theory used for calculating the corrections (Györgyi et al. 2008, 2010).

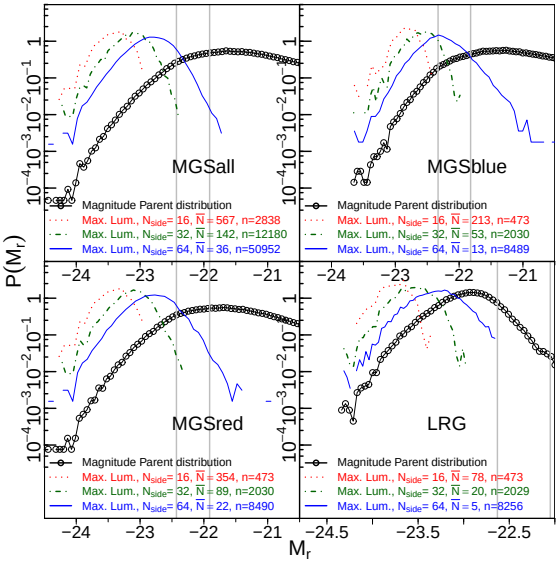

Figure 12. Parent distribution of r-band absolute magnitude M_r for the full samples. Also included are the distribution of the maximal luminosity for each sample according to different HEALPix resolutions. The vertical lines show the points where $w_i = 1$ (left line) and $w_i = 2$ (right line).

6.2. *Statistics from HEALPix-based batches*

The distributions of the maximal luminosities (in magnitude space) for the HEALPix-based method are shown in Fig. 12. Here, the low luminosity tails of the maximal distributions reach farther into the low luminosity regions (around $M_r \simeq M_D$) than in the random sampling method. The reason is that some of the HEALPix cells have very low values of N. The maximal luminosities, however, are mostly sampled in the region where $w_i \lesssim 2$. As this is the high luminosity region where the LD and LF mostly coincide, all the results obtained from analyzing the bright end of the LD can be also extended and associated with the LF.

Fig. 13 presents the distributions of maximal luminosities (in luminosity space) observed in a HEALPix cell for the three studied resolutions ($N_{side} = 16, 32, 64$) and for the four galaxy populations. The distributions on this figure are scaled to zero mean and unite deviation in order to compare them with the similarly scaled Gumbel distribution. The theoretical first order correction coming from the finite-size (finite N) effects, together with the correction to the i.i.d. limit distribution coming from the distribution $\mathcal{F}(N)$ of the galaxy counts are also shown on Fig. 13. Except for the cases of $N_{side} = 16$, where the statistical noise has larger amplitude than the

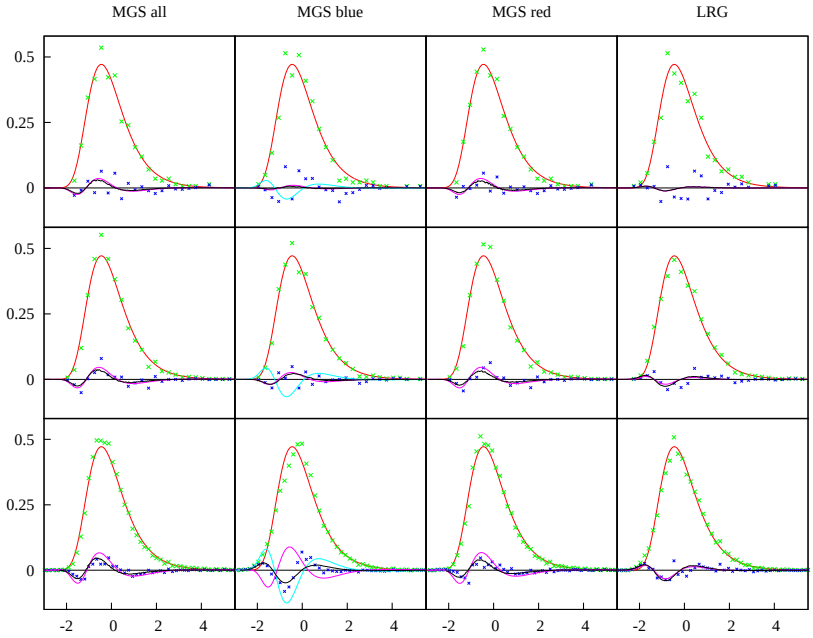

Figure 13. The normalized maximum luminosity histograms (green crosses) for $N_{side} = 16$, 32, 64 (from up to down) for the four galaxy samples compared to the limit distribution FTG (solid red line) in scaled variables ($\langle x \rangle = 0$ and $\sigma = 1$) while blue crosses are the residuals to the FTG. For the MGS, the solid magenta curves show $q(N)P_1(x) + \overline{P}_1(x)$, i.e., the first order finite size correction for the Schechter parent added to the variable batch size correction calculated for (18). The LRG curve is different, in the sense that the parent is FTG and the finite size corrections do not appear, having corrections only due to the variable batch size ($\overline{P}_1(x)$). The light blue curves show the finite-size correction calculated using the fitting parameters of the LD for MGSblue. The black solid curves are the simulations that result from using the experimentally given luminosity distributions and sample size distributions.

corrections, it appears that the sum of this two corrections is of the order of the residuals and have the same functional shape. At the highest order resolution of the maps ($N_{size} = 64$), however, the batch sizes are rather small and the finite-size corrections become large.

As can be seen from Fig. 13, well defined shape corrections emerge which are in accord with the theoretical predictions. The case of the $N_{side} = 64$ MGSblue sample needs, however, special considerations. Here the $\bar{N} = 13$ case displays the same behavior as in the random sampling schema in Sec. 6.1.2 for $N = 12$, where the sign of the correction appeared to be inverted with respect to the theoretical corrections. As we can observe in Fig. 12, the maximal luminosities for MGSblue ($N_{side} = 64$) do reach much farther into the low luminosity tail than the other samples, and the peak is placed exactly at the $w_i = 1$ departure boundary between the LF and LD. It follows then that the values of α and β from the LD give the right sign to the correction, as opposed to the parameters from the LF fitting, as can indeed be seen on Fig.13.

The LRGs are special in the sense that finite size effects do not emerge in their EVS, because the parent distribution itself is Gumbel, as explained in 5.2.1. Consequently the only correction to the limit distribution comes from the variable batch size N, in agreement what we see in the fourth column in Fig. 13.

We carried out simulations as well in order to confirm our theoretical results by modeling the empirical situation with less noise. Sampling the fitted functions of the empirical parent and sample size distributions with high statistics ($n = 10^7$) we get smoother histograms. As can be seen on Fig. 13, the simulated corrections are indeed a good model for the empirical corrections, and support the theoretical expectations as we can observe the convergence toward the theoretical curve for increasing $\overline{N}$.

7. DISCUSSION AND CONCLUSION

Studying extreme statistics may have several outcomes. One may discover that the objects under consideration have a well defined i.i.d. type extreme value distribution. This may then lead to the conclusion (provided the distribution is of the Weibull type - i.e. the shape parameter is negative) that the underlying objects have an intrinsic cutoff in size. In our case the luminosities have an i.i.d. EVS, but the shape parameter ξ is in the positive range and very close to zero. Thus our conclusion here is that the MGS and LRG luminosities do not have an upper cutoff.

As far as the LRGs are concerned, we should note that the same conclusion about the absence of an upper cutoff can be reached by a straightforward fit to the high end of the luminosity function. On the other hand, there are difficulties with the agreement of the Schechter fitting to the bright end of the MGS LF (e.g. Madgwick et al. 2002; Bell et al. 2003; Blanton et al. 2003; Smith et al. 2009). Here the EVS analysis suggests that the root of the problem may be a small positive tail parameter ξ. This possibility was also noted by Alcaniz & Lima (2004) with their proposal of the generalized double power law fitting function for the LF.

Of course, the conclusion that MGS galaxies do not have a finite luminosity cutoff and ξ has a small positive

value is valid only if the methods used in the study are robust against possible corrections arising in the analysis. Uncertainties may come from the finite size of the sample, from the distribution of the number of objects in the sample, and from the correlations among the objects. We have taken care of the finite-size effects by including the first order corrections in the limit distributions and, furthermore, we handled the fluctuations in the sample size by explicitly calculating their effect for the i.i.d. case.

As evidenced by Figs. 11 and 13, a parameter free comparison with the data suggests good agreement with the corrections (for the case $\xi = 0$) being the right order of magnitude as well as of the right shape. Thus, we believe that the above effects are in agreement with the conclusion about the absence of upper cutoff in the luminosity. Of course, the agreement proved to be valid when the fitting parameters come from a parent distribution fitted in the high luminosity tail, as expected from the theory. If the batch size N decreases and the peak of the maximal luminosities moves into the lower luminosity region, agreement with theory is obtained only if the fitting is performed in an extended luminosity interval considering the lower luminosity values.

The correlations pose a more difficult problem. For one dimensional systems, it is known from the studies of $1/f^{\alpha}$ type signals that the correlations are irrelevant if they are "weak" (Györgyi et al. 2007). Weak means that the integral of the correlation function is finite. The effectively one-dimensionality of the pencil beam geometry considered in this paper allows the application of the weakness criteria for the luminosity correlations. Indeed, one may argue that the luminosity correlations $C_L(r)$ are proportional to the density correlations $C_\rho(r)$ which, at large distances decay as $C_L(r) \sim C_\rho(r) \sim 1/r^2$. The one-dimensional integral of this type of correlations is convergent, thus we believe the weakness criteria is satisfied, and our conclusion is not affected by the correlations [note that any power relationship between the correlations ($C_L(r) \sim C_\rho^{\mu}(r)$) will also satisfy the criteria of weakness provided $\mu > 1/2$].

We can thus conclude that the extreme value statistics of galaxy luminosities is i.i.d. type with zero or small positive shape parameter, and this conclusion takes into account the finite-size of the samples, the galaxy-number fluctuations in the pencil beams, and the large-distance spatial correlations among luminosities.

K. O. and Z. R. have been partially supported by the Hungarian Science Foundation OTKA through grants No. K 68109 and NK100296. M.T.P thanks Ching-Wa Yip and Mark Neyrinck for useful discussion.

Funding for SDSS-III has been provided by the Alfred P. Sloan Foundation, the Participating Institutions, the National Science Foundation, and the U.S. Department of Energy Office of Science. The SDSS-III web site is http://www.sdss3.org/.

SDSS-III is managed by the Astrophysical Research Consortium for the Participating Institutions of the SDSS-III Collaboration including the University of Arizona, the Brazilian Participation Group, Brookhaven National Laboratory, University of Cambridge, Carnegie Mellon University, University of Florida, the French Participation Group, the German Participation Group, Harvard University, the Instituto de Astrofisica de Canarias, the Michigan State/Notre Dame/JINA Participation Group, Johns Hopkins University, Lawrence Berkeley National Laboratory, Max Planck Institute for Astrophysics, New Mexico State University, New York University, Ohio State University, Pennsylvania State University, University of Portsmouth, Princeton University, the Spanish Participation Group, University of Tokyo, University of Utah, Vanderbilt University, University of Virginia, University of Washington, and Yale University.

REFERENCES

Aihara, H., et al., 2009, ApJS, 193, 29A
Alcaniz, J. S. & Lima, J.A.S. 2004, Brazilian Journal of Physics, 34, 2A
Baldry, I. K., et al. 2004, ApJ, 600, 681
Bell, E. F., McIntosh, D. H., Katz, N., & Weinberg, M. D. 2003, ApJS, 149, 289
Berman S. M., Ann. Math. Stat. 33, 502 (1964).
Bhavsar, S. P. & Barrow, J. D. 1985, MNRAS, 213, 857
Binggeli, B., Sandage, A. & Tammann, G.A. 1988, ARA&A, 26, 509
Blanton, M. R., Dalcanton, J., Eisenstein, D., et al. 2001, AJ, 121, 2358
Blanton, M. R., Hogg, D. W., Bahcall, N. A., et al. 2003, ApJ, 592, 819
Bruzual A.,G. & Charlot ,S., 2003, MNRAS 344, 1000
Budavári, T., et al., 2000, AJ, 120, 1588
Csabai, I., Connolly, A. J., Szalay, A.S., & Budavári, T. 2000, AJ, 119,69
Cooray, A. & Milosavljevic, M. 2005, ApJ, 627, L89
Cooray, A. 2006, MNRAS, 365, 842
De Lucia G. & Blaizot J. 2007, MNRAS, 375, 2
Dobos, L. & Csabai, I. 2011, MNRAS, 414, 1862D
Eisenstein, D., et al. 2001, ApJ, 122, 2267
Fioc, M., & Rocca-Volmerange, B. 1997, A&A, 326, 950
Galambos, J. 1978, The Asymptotic Theory of Extreme Order Statistics (New York: Wiley)
Geller, M. J. & Peebles, P. J. E. 1976, AJ, 206, 939
Górski, K. M., et al. 2005, ApJ, 622, 759
Gumbel, E. 1958, Statistics of Extremes (New York: Dover).
Györgyi, G., Moloney, N. R., Ozogány, K. and Rácz, Z. 2007, Phys. Rev. E 75, 021123
Györgyi, G., Moloney, N. R., Ozogány, K. and Rácz, Z. 2008, Phys. Rev. Lett. 100, 210601
Györgyi, G., Moloney, N. R., Ozogány, K., Rácz, Z. and Droz, M. 2008, Phys. Rev. E , 81, 041135
Lin, Y. et al. 2010, ApJ, 715, 1486
Loh, Yeong-Shang 2004, Luminous Red Galaxies in the Sloan Digital Sky Survey, Princeton Physics PhD thesis.
Loh, Yeong-Shang & Strauss, M. A. 2006, MNRAS366, 373
Madgwick, D. S. et al. 2002, MNRAS, 333, 133
Ostriker J. P. & Hausman M. A., 1977, ApJL, 217, L125
Paranjape, A. & Sheth, R. K. 2011, arXiv:1107.3652
Postman, M. & Lauer, T. R. 1995, ApJ, 440, 28
Press,W. H. & Schechter, P. 1974, ApJ, 187,425
Schechter, P. 1976, ApJ, 203,297
Schmidt, M. 1968, ApJ, 151, 393
Shimazaku, K., et al. 2001, AJ, 122, 1238
Smith, A. J., et al. 2009, MNRAS, 397, 868
Stoughton, C., Lupton, R. H., Bernardi, M., et al. 2002, AJ, 123, 485
Strateva, I., et al., 2001, AJ, 122, 1861
Strauss, M. A., et al. 2002, AJ, 124, 1810
Taghizadeh-Popp, M. 2010, PASP, 122, 976
Tremain, S. D. & Richstone, D. O. 1977, AJ, 212, 311
York, D. G., et al. 2000, AJ, 120, 1579